European Journal of Mechanics B/Fluids 38 (2013) 93–100

Contents lists available at SciVerse ScienceDirect

European Journal of Mechanics B/Fluids

journal homepage: www.elsevier.com/locate/ejmflu

Convective and absolute instabilities in the boundary layer over rotating spheres with surface mass flux and incident axial flow

A. Barrow, S.J. Garrett *

Department of Mathematics, University of Leicester, UK

ARTICLE INFO

Article history:
Received 13 June 2012
Received in revised form
3 October 2012
Accepted 9 October 2012
Available online 14 November 2012

Keywords:
Boundary-layer flow
Rotating sphere
Mass flux
Axial flow

ABSTRACT

We consider the effect of surface mass flux and forced axial flow on the boundary-layer flows over rotating spheres, with a view to establishing flow-control mechanisms for rotating flows of engineering significance. A theoretical study is presented which considers the onset of convective instability modes (both stationary and travelling relative to the rotating surface) and local absolute instability. Suction is found to be universally stabilising in terms of the delayed onset of both instability types. Extensive theoretical data are presented for future comparison to experiments.

1. Introduction

Many applications in fluid mechanics have shown that surface suction can be used as an effective flow-control mechanism. For example, Gregory and Walker [1] discuss how the introduction of suction extends the laminar-flow region over a swept wing by reducing the thickness of the boundary layer and the magnitude of crossflow velocity. Conclusions for the swept-wing flow arose from equivalent studies of the von Kármán (rotating disk) flow (see Gregory and Walker [2], Stuart [3]) and work has since continued into this and related flows using numerical and asymptotic approaches (see Ockendon [4], Dhanak [5], Bassom and Seddougui [6], Lingwood [7], Turkyilmazoglu [8], Lingwood and Garrett [9], for example). The literature shows that increasing suction has a stabilising effect on the general class of "Bödewadt, Ekman and von Kármán" (BEK) flows which results in an increase in critical Reynolds numbers for the onset of convective and absolute instabilities, a narrowing in the range of unstable parameters and a decrease in amplification rates of the unstable convective modes. The convective instability results are interpreted in terms of a delay in the onset of spiral vortices, and the absolute instability results in terms of the onset of laminar-turbulent transition (Lingwood [7,10,11]).

Garrett and Peake [12–14] have demonstrated the close connection between the von Kármán flow and the steady boundary-layer flow over a rotating sphere, particularly at latitudes close to the pole, where the sphere is locally flat. They find that convective and absolute instability exist on the sphere as with the disk, with increasing discrepancies at higher θ owing to the local curvature of the surface. Although the implications of suction have been extensively studied for the von Kármán flow, we are unaware of any studies for the flow over rotating spheres which have direct practical relevance in engineering applications. This is addressed in this paper. In particular, we perform a stability analysis on the boundary-layer flow over a rotating sphere subject to surface mass flux and forced axial flow, extending the literature in this area.

The laminar boundary-layer flow over rotating spheres has been the subject of previous research. Howarth [15], and later Banks [16], use a series-solution method to calculate the steady flow as a function of latitudinal position for spheres rotating in otherwise still fluid. Further theoretical studies (Manohar [17], Banks [18]) apply more accurate finite-difference techniques to the same problem. More recently, Garrett and Peake [12–14] apply an efficient and commercially available numerical scheme to obtain the steady flow for spheres rotating in otherwise still fluid and a forced axial flow - this will be the approach taken here.

In Section 2, we generalise the governing partial differential equations (PDEs) presented in the literature for the boundary-layer flow over a rotating sphere to include both surface mass flux and forced axial flow. The resulting equations are then solved at each latitude. The effects of altering the incident axial flow speed and mass flux are discussed. Our results for the case of zero mass-flux show excellent agreement with those of Garrett and Peake [13,14].

In Section 3 we present stability analyses for both convective and absolute instabilities for a range of flow parameters. Conclusions are drawn in Section 4. In particular, the implications of these

* Corresponding author. Tel.: +44 0 116 252 3899.
E-mail addresses: s.garrett@mcs.le.ac.uk, sjg50@le.ac.uk (S.J. Garrett).

0997-7546 © 2012 Elsevier Masson SAS. Open access under CC BY license.
doi:10.1016/j.euromechflu.2012.10.010

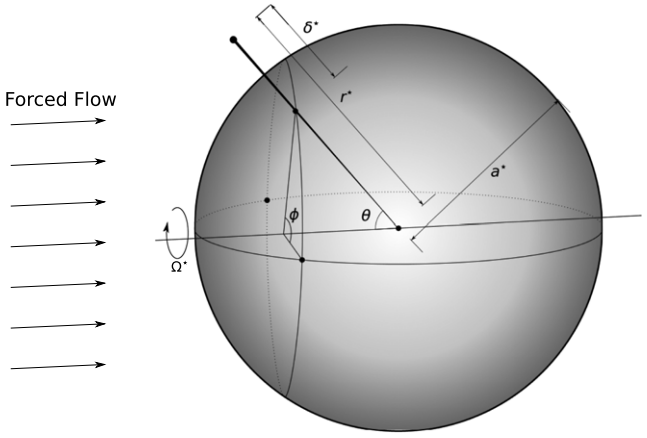

Fig. 1. Coordinate system used throughout this work.

results in the context of engineering applications, for example, hemispherical nose cones occurring in projectile and aeroengine applications, are discussed.

2. Steady basic flow

2.1. Formulation

This work is concerned with the local linear stability of the boundary-layer flow around a rotating sphere immersed in an incompressible viscous fluid. The formulation is closely related to previous work by Garrett and Peake [12–14], but it is summarised here for completeness.

The sphere, of radius $a^\star$, rotates around its axis with angular velocity $\Omega^\star$ (dimensional quantities are indicated by *). We use a spherical coordinate system centred on the sphere and fixed in space (see Fig. 1), here $r^\star$ is the radial distance from the centre of the sphere, θ is the angle of latitude measured from the pole, and ϕ is the angle of azimuth measured from some fixed plane parallel to the axis of rotation. The quantities $U^\star$, $V^\star$ and $W^\star$ are the velocity components of the basic steady flow in the θ, ϕ and $r^\star$ directions, respectively. $P^\star$ is the pressure. The kinematic viscosity of the surrounding fluid is $\nu^\star$, and the boundary-layer thickness is denoted by

$$\delta^\star = \left(\frac{\nu^\star}{\Omega^\star}\right)^{\frac{1}{2}} \ll 1.$$

The following scalings are used to to non-dimensionalise the steady-flow quantities:

$$U(\eta,\theta) = \frac{U^\star}{\Omega^\star a^\star}, \qquad V(\eta,\theta) = \frac{V^\star}{\Omega^\star a^\star},$$
$$W(\eta,\theta) = \frac{W^\star}{(\nu^\star\Omega^\star)^{1/2}},$$

where $\eta = \left(\frac{\Omega^\star}{\nu^\star}\right)^{\frac{1}{2}}(r^\star - a^\star)$ is the non-dimensional distance from the sphere surface. It is then natural to define the Reynolds number as $R = a^\star\delta^\star\Omega^\star/\nu^\star$. This formulation means that for a fixed sphere radius and fluid viscosity, R is simply a function of $\Omega^\star$ and it can be interpreted as the rotation rate of the sphere. This is in contrast to similar studies on the rotating disk (Lingwood [7], for example), where R is interpreted as radial position. For the sphere the position of the local analysis is given by the latitude, θ.

Two assumptions are made: firstly, that the steady flow has rotational symmetry, so that we can neglect azimuthal variation; secondly, that the boundary layer is locally spatially homogeneous. The second assumption is sometimes called the "parallel flow" assumption, and amounts to assuming that $\eta/R \approx 0$ in some instances. This simplifies the governing equations, but will limit the stability analyses to a "local" analysis at particular positions on the sphere surface. The governing steady Navier–Stokes equations are derived in terms of our scaled variables.

To impose an incident axial flow, we introduce $U^\star_\infty$ as the dimensional free-stream speed of incident axial flow, and define an axial-flow parameter $\tau = U^\star_\infty/a^\star\Omega^\star$, relative to the speed of the sphere surface at the equator. Following Garrett and Peake [13,14], the form of the free-stream velocity is given by the empirical results of Fage [19], Eq. (5), and this enables us to form an explicit expression for the stream-wise gradient of the steady pressure within the Navier–Stokes equations.

To impose a non-zero surface mass flux, we introduce $\iota^\star$ as the dimensional mass-flux parameter, representing the mass flux through the sphere surface. This is modelled by a simple change to the boundary condition for the normal velocity component: $W^\star(0) = \iota^\star$ on the surface of the sphere which is scaled as

$$\iota = \frac{\iota^\star}{(\nu^\star\Omega^\star)^{1/2}} = \iota^\star\frac{R}{a^\star\Omega^\star}.$$

We note that the mass-flux parameter is related to the equatorial surface speed, but scaled on the Reynolds number that otherwise does not appear in the steady flow system. That the scaling of the mass-flux parameter depends only on global properties of the system (not latitudinal location), means that a particular ι can be used to represent the same mass-flux at all latitudes over the sphere.

The governing steady-flow equations, after carrying out the boundary-layer approximation, are then written as

$$W\frac{\partial U}{\partial\eta} + U\frac{\partial U}{\partial\theta} - V^2\cot\theta = \tau^2 U_0\frac{dU_0}{d\theta} + \frac{\partial^2 U}{\partial\eta^2}, \tag{1}$$

$$W\frac{\partial V}{\partial\eta} + U\frac{\partial V}{\partial\theta} + UV\cot\theta = \frac{\partial^2 V}{\partial\eta^2}, \tag{2}$$

$$\frac{\partial W}{\partial\eta} + \frac{\partial U}{\partial\theta} + U\cot\theta = 0. \tag{3}$$

subject to boundary conditions

$$\begin{aligned} &U = V - \sin\theta = 0, \qquad W = \iota \quad \text{on } \eta = 0,\\ &V = U - \tau U_0 = 0 \quad \text{as } \eta \to \infty. \end{aligned} \tag{4}$$

The distribution of the outer flow, based on the results of Fage [19], is given by

$$U_0(\theta) \approx 1.5\theta - 0.4371\theta^3 + 0.1481\theta^5 - 0.0423\theta^7, \tag{5}$$

with θ in radians. We consider the parameters to be in the range $0 \le \tau \le 0.25$ (consistent with Garrett and Peake [13,14]) and $-1 \le \iota \le 1$. These ranges are arbitrarily imposed to limit the number of cases to be studied, but can be extended within this formulation.

2.2. Steady-flow profiles

Eqs. (1)–(3) are solved subject to boundary conditions (4) using a numerical routine, commercially available from the Numerical Algorithms Group, as discussed by Garrett and Peake [12–14]. The results are shown in Figs. 2–4, where the combined effects of incident axial flow and surface mass flux can be seen. In each figure, profiles are arranged in a 3×3 grid, with rows corresponding to latitudes $\theta = 10^\circ, 40^\circ$ and 70°. The central column corresponds to zero mass flux, while the left and right columns show example cases of suction and injection, respectively. Within each set of axes,

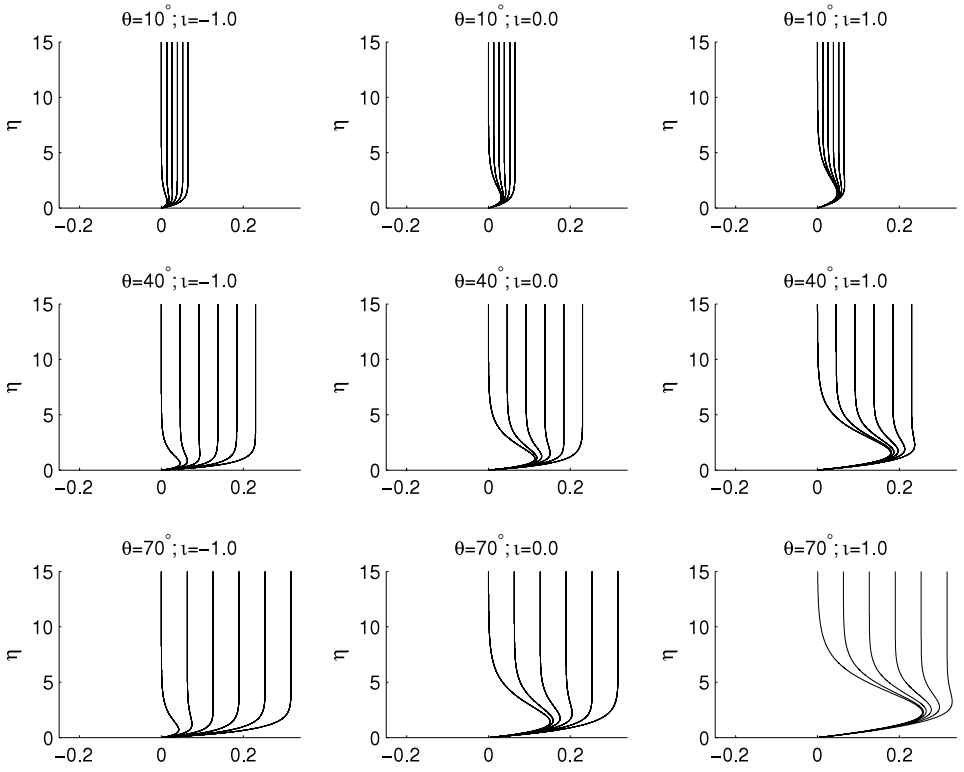

Fig. 2. Latitudinal velocity (U) profile for latitudes of $\theta = 10^\circ, 40^\circ, 70^\circ$ (rows, top to bottom); for $\iota = -1, 0, 1$ (columns, left to right) for $\tau = 0$ to 0.25 in intervals of 0.05 (lines, left to right).

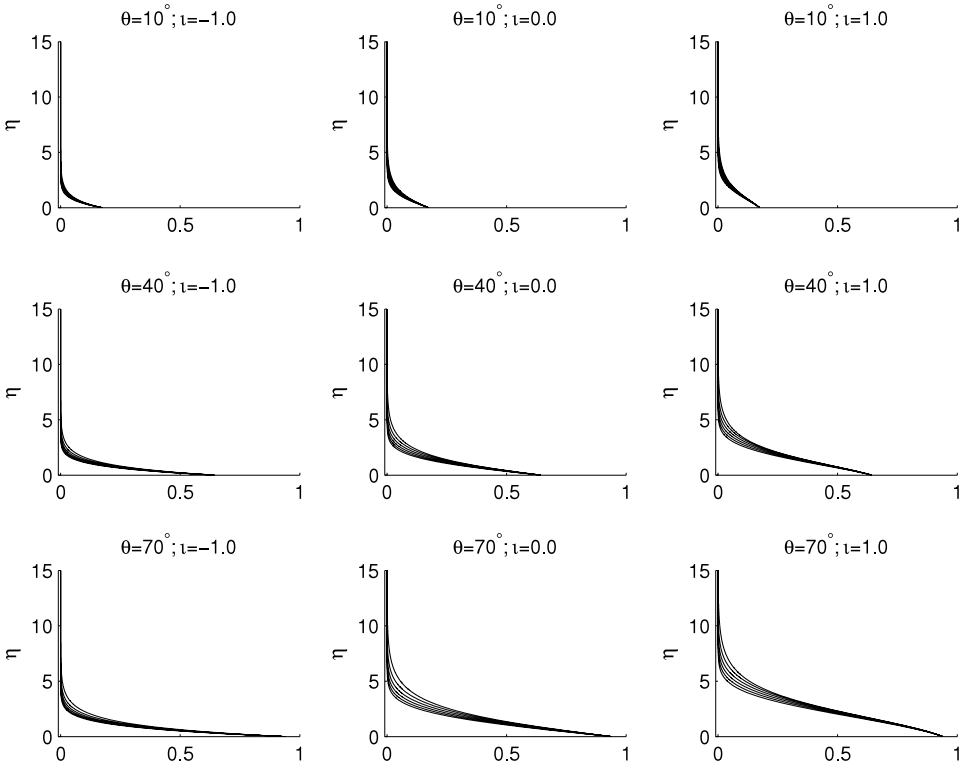

Fig. 3. Azimuthal velocity (V) profile for latitudes of $\theta = 10^\circ, 40^\circ, 70^\circ$ (rows, top to bottom); for $\iota = -1, 0, 1$ (columns, left to right) for $\tau = 0$ to 0.25 in intervals of 0.05 (lines, left to right).

there are six lines, read left to right, corresponding to $\tau = 0$ to $\tau = 0.25$ in intervals of 0.05. We note that profiles are identical to those in literature (Garrett and Peake [12–14]) for appropriate parameter values.

Examining Fig. 2, we see that increased axial flow causes U to tend to a larger constant value at each latitude, as would be expected. It has a much greater effect on the streamwise flow component at higher latitudes. Mass flux does not alter the value

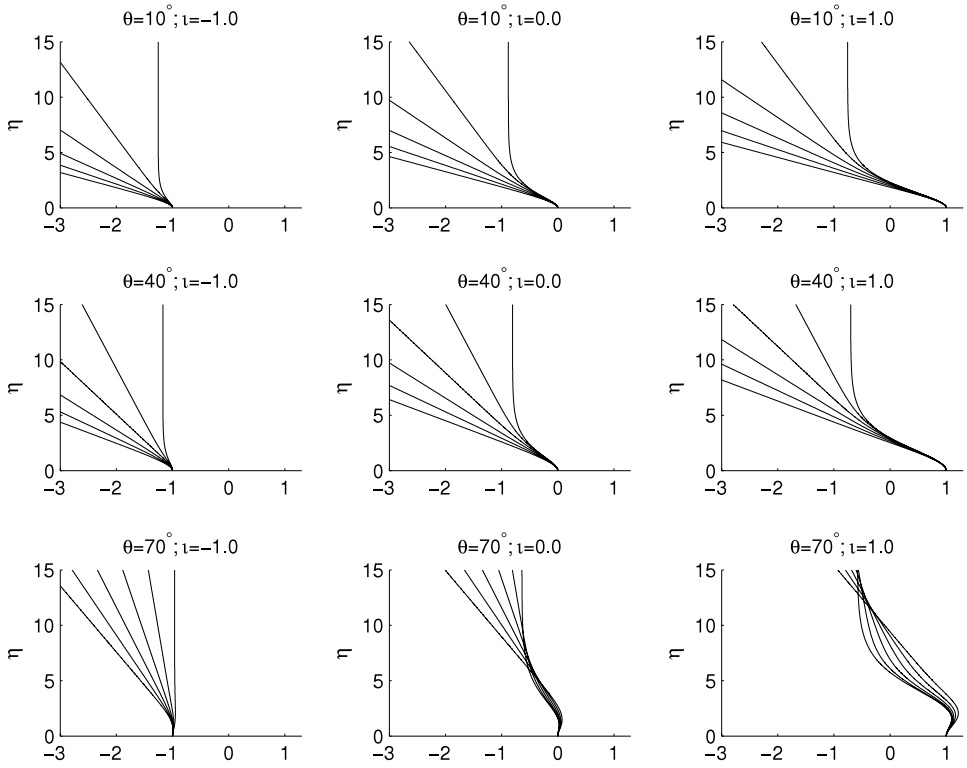

Fig. 4. Azimuthal velocity (W) profile for latitudes of $\theta = 10°, 40°, 70°$ (rows, top to bottom); for $\iota = -1, 0, 1$ (columns, left to right) for $\tau = 0$ to 0.25 in intervals of 0.05 (lines, lower-left to right).

to which U tends in the far field, though it does affect the profile close to the sphere surface. The distortion of the wall jets caused by mass flux is significantly reduced by increased rates of axial flow. This can be seen from the figure by observing that across any row, the left-most line undergoes a much larger change than the right-most.

Increasing axial flow has a less pronounced effect on V, but it clearly causes it to maintain a lower magnitude close to the sphere surface, eventually tending to the same constant value as $\eta \to \infty$. This is shown in Fig. 3. Similarly to the case for U, the effect is greater at higher latitudes. Mass flux appears to have a small effect, slightly magnifying the effects of axial flow.

It can be seen from Fig. 4 that non-zero forced axial flow prevents W from tending to a constant value with increasing η, and instead causes it to assume a constant rate of change as $\eta \to \infty$. This implies that fluid is entrained into the boundary layer at unbounded speed as $\eta \to \infty$. As noted by Garrett and Peake [13,14,20], this is a consequence of the boundary-layer approximations used in the model; it is clearly impossible for the fluid to maintain this acceleration at an indefinite distance from the sphere. However, the scalings are such that W appears at a lower order of magnitude than U and V and the effects are not significant. The effects of axial flow *decrease* with increasing latitude.

The effects of each parameter on the boundary-layer thickness are not measured, but it can be seen from Fig. 3 that the boundary layer thickens slightly with increased θ. Surface suction and injection significantly thin and thicken the boundary layer, respectively, and increased τ is seen to have a minor thinning effect.

3. Stability analyses

The formulation used in this study is such that effects of forced axial flow and surface mass flux are contained in the steady-flow profiles discussed in Section 2.2. The unsteady perturbation equations for the system are therefore identical to those used by Garrett and Peake [12] and are listed as Eqs. (2.13)–(2.18) of that paper, where details of their derivation can also be found, including a discussion of the parallel-flow type approximation made. Here it is sufficient to understand that the approximation limits the analysis to a local analysis at each value of θ and means that the governing equations are not entirely rigorous at $O(R^{-1})$.

The perturbation equations are derived by imposing unsteady perturbations of normal mode form given by

$$(\hat{u}, \hat{v}, \hat{w}, \hat{p}) = (u(r), v(r), w(r), p(r))e^{\mathrm{i}(\alpha\theta+\beta\phi\sin\theta-\gamma t)}.$$

The wavenumber in the θ-direction and frequency are complex quantities, $\alpha = \alpha_r + \mathrm{i}\alpha_i$ and $\gamma = \gamma_r + \mathrm{i}\gamma_i$, to enable the spatio-temporal analyses presented later; the azimuthal wavenumber, β, is real. Each of these perturbing quantities is added to its corresponding steady flow variable.

The unsteady perturbation equations are subject to boundary conditions that restrict the perturbations to the boundary-layer region; the resulting system forms a dispersion relation that is parametrised by the Reynolds number, location of the analysis and the flow parameters, $D(\alpha, \beta, \gamma; R, \theta, \tau, \iota) = 0$. The dispersion relation can now be solved to compute the branches that dictate the stability properties of the flow.

Note that throughout this work, we make the assumption that the perturbations are small enough so that a linear analysis is sufficient, i.e., nonlinear effects can be neglected.

3.1. Convective instabilities

We begin by supposing that the flow is not absolutely unstable and, in the Briggs–Bers [21] procedure, we can reduce the imaginary part of the frequency to zero, so that $\gamma_i = 0$. We proceed by insisting that the disturbances rotate at some fixed multiple of the sphere surface velocity, thereby fixing the ratio γ/β. The non-dimensional speed of the sphere surface is $\sin\theta$, and equating the

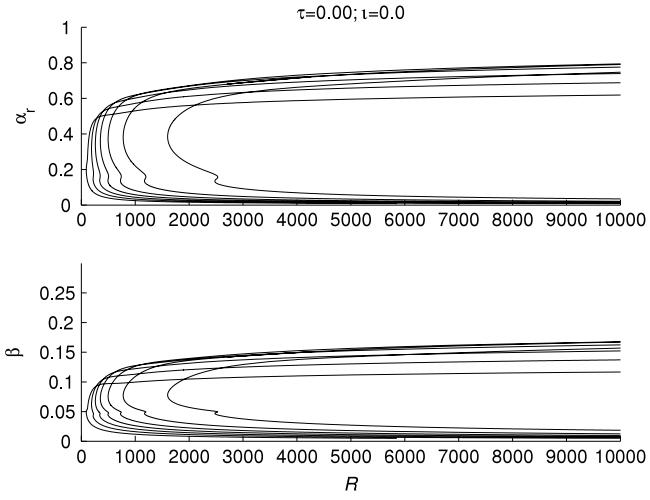

Fig. 5. Neutral-stability curves for α_r and β at $\tau = 0$, $\iota = 0$ (still fluid), and $\theta = 10^\circ$ to 70° in intervals of 10° (right to left).

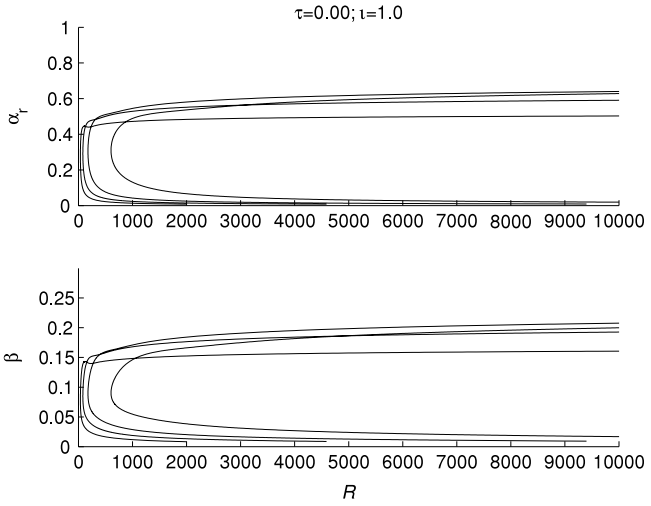

Fig. 6. Neutral-stability curves for α_r and β at $\tau = 0, \iota = 1.0$, and $\theta = 10^\circ, 30^\circ, 50^\circ, 70^\circ$ (right to left).

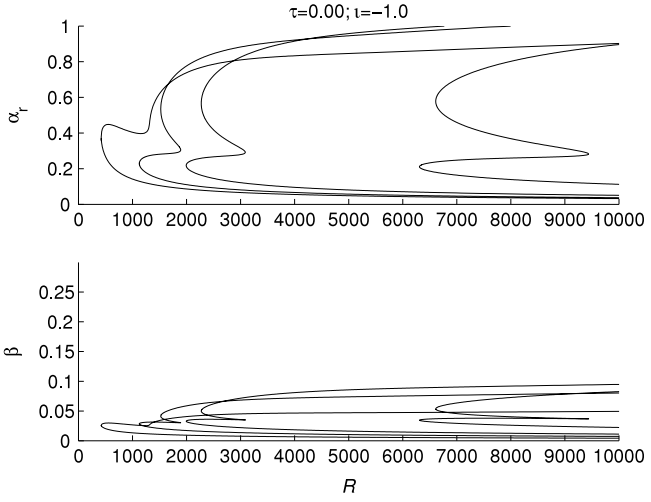

Fig. 7. Neutral-stability curves for α_r and β at $\tau = 0, \iota = -1.0$, and $\theta = 10^\circ, 30^\circ, 50^\circ, 70^\circ$ (right to left).

relevant multiple of this with the disturbance phase velocity in the same direction, γ/β, leads to $\gamma = c\beta\sin\theta$. This relationship must be satisfied with $c = 1.0$ if the vortices are to rotate with the sphere, and $c = 0.76$ if the vortices are those experimentally reported by Kobayashi and Arai [22], for example. This approach reduces the dispersion relationship to

$$D(\alpha, \beta, \gamma = c\beta\sin\theta; R, \theta, \tau, \iota) = D(\alpha, \beta; R, \theta, c, \tau, \iota) = 0.$$

Having fixed the value of c, we can march through β and R to map spatial branches in the complex α plane for particular values of τ and ι. We form neutral curves by taking the points at which these branches intersect the real axis, for a range of R. This method was denoted as *method* 2 by Garrett [14,23].

In this convective analysis, $-\alpha_i$ is interpreted as the spatial growth rate. Furthermore, the angle that the phase fronts make with a circle parallel to the equator is denoted ϵ, and it is clear that $\epsilon = \arctan(\beta/\alpha_r)$. The integer number of complete cycles of the disturbance round the azimuth is $n = \beta R\sin\theta$. The quantities ϵ and n can then be identified with the angle and number of spiral vortices on the sphere surface, respectively.

As in previous studies published in the literature (Garrett and Peake [12–14]), two branches were found to dictate the convective instability properties of the flow at all parameter values. These are known to arise from inviscid crossflow instabilities (type I branches) and viscous streamline-curvature instabilities (type II branches).

Stationary vortices

We set $c = 1$, so that the vortices are stationary with respect to the sphere surface. Presented here is a small selection of neutral-stability curves in the R-α_r and R-β planes. The curves typically exhibit two lobes: the upper, which occurs at higher streamwise wavenumbers, arises due to the type I (crossflow) mode; and the lower, which occurs at lower streamwise wavenumbers, arises due to the type II (streamline-curvature) mode. We use the critical Reynolds number, R_c, as a quantitative measure of the stability of a system. In cases where two lobes are present, the one which extends to the smallest Reynolds number (i.e., the one which determines R_c) is identified with the dominant instability mode.

Figs. 5–7, show example cases of zero, positive and negative surface mass flux, all without forced axial flow, at various latitudes. Fig. 9 examines in detail the case of $\theta = 30^\circ$, showing the behaviour of R_c as τ and ι are varied.

In all cases, increased suction exaggerates the two-lobe profile of the curve and indicates higher critical Reynolds numbers, and a larger stable region overall. This is to be expected, since suction has been seen to have a stabilising influence in similar models (see the work by Lingwood and Garrett [7,9] on the BEK system, for example). The type II mode becomes dominant as suction is increased. Injection has the opposite effect, and we see that the two-lobe form is lost for high magnitudes with the type I remaining dominant (see Fig. 8, for example). For the case of $\iota = 0$, our results agree with those of Garrett and Peake [13].

Increasing the magnitude of forced axial flow, τ, increases the relative importance of the streamline-curvature lobe. It also moves both the upper and lower branches to larger wavenumbers for large R, but the effect on the upper branch is much greater, so convective instability can occur over a wider range of wavenumbers. Small magnitudes of forced axial flow decrease the critical Reynolds number of the type II lobe, and at high latitudes (with the precise value depending on ι), where the type II lobe is dominant, this results in a lower value for R_c. Thus, in these cases, moderate axial flow is seen not only to broaden the unstable range of wavenumbers, but also to cause a small decrease in R_c, making the model more susceptible to instability. Further increasing τ, however, increases R_c, and the behaviour becomes typical of that seen at lower latitudes. The threshold value of τ, above which R_c surpasses its value at $\tau = 0$, is dependent on the latitude and ι. Both surface mass injection and suction reduce the magnitude of this effect, and it is not observed at all with strong suction.

Table 1
R_c for $\tau = 0.00$. Two Reynolds numbers are given where two lobes are present. Values for Type II lobes are in parentheses. The dominant mode (i.e. lowest critical Reynolds number) is bold. A dash indicates missing data.

ι	θ			
	10°	30°	50°	70°
−1.0	6610.6 (**6309.1**)	2272.4 (**1993.5**)	1523.0 (**1127.0**)	(**421.2**)
0.0	**1601.5** (2478.0)	**497.2** (726.0)	**260.7** (341.8)	(**92.3**)
1.0	(**602.7**)	(**176.9**)	(**82.0**)	(**36.3**)

Table 2
R_c for $\tau = 0.10$. Bold values and values in brackets follow convention of Table 1.

ι	θ			
	10°	30°	50°	70°
−1.0	9705.7 (**8350.7**)	–	2187.4 (**1469.4**)	–
0.0	**2117.0** (2494.6)	**655.6** (724.4)	340.9 (**329.9**)	(**71.7**)
1.0	(**664.2**)	(**193.4**)	(**88.0**)	(**37.4**)

Table 3
R_c for $\tau = 0.25$. Bold values and values in brackets follow convention of Table 1.

ι	θ			
	10°	30°	50°	70°
−1.0	–	–	–	–
0.0	3541.6 (**3448.2**)	1116 (**1010**)	598.5 (**473.4**)	(**119.5**)
1.0	(**973.3**)	(**285.3**)	(**130.7**)	(**55.9**)

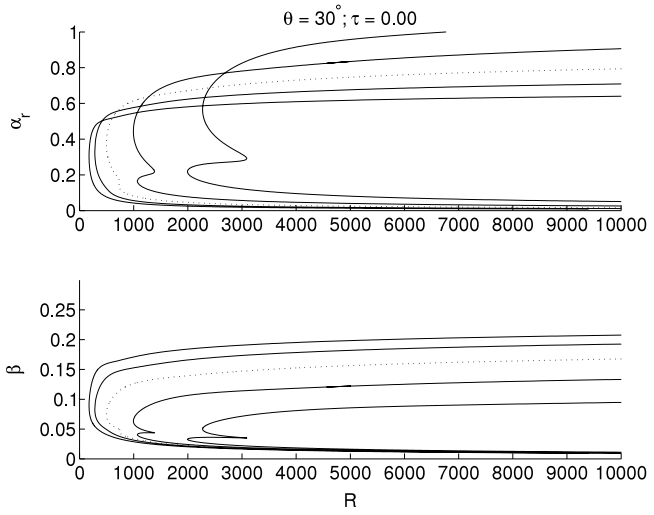

Fig. 8. Neutral-stability curves for α_r and β at $c = 1.00, \theta = 30°$, for $\iota = -1, -0.5, 0, 0.5, 1$ (leftmost-top to bottom).

Tables 1–3 show the computed critical Reynolds numbers for a representative range of parameters. Where the neutral curve has two lobes, a critical Reynolds number is given for each lobe. The type I lobe is always presented first, if present, and the type II is given in parentheses. The dominant mode (i.e. lowest critical Reynolds number) is given in bold text. A dash in the table indicates a combination of parameter values for which no data could be obtained.

Non-stationary vortices

We now consider vortices which travel at speeds slower than the local sphere surface and have $c \neq 1$. Slow vortices ($c < 1$) were observed experimentally by Kobayashi and Arai [22] and have been studied by Garrett [14] in the case of zero surface mass flux. They are expected to be important over highly-polished surfaces. However, for completeness we also present results for $c > 1$.

Fig. 10 shows a still-fluid example of how neutral-stability curves vary over a range of c at a latitude of $\theta = 30°$. They

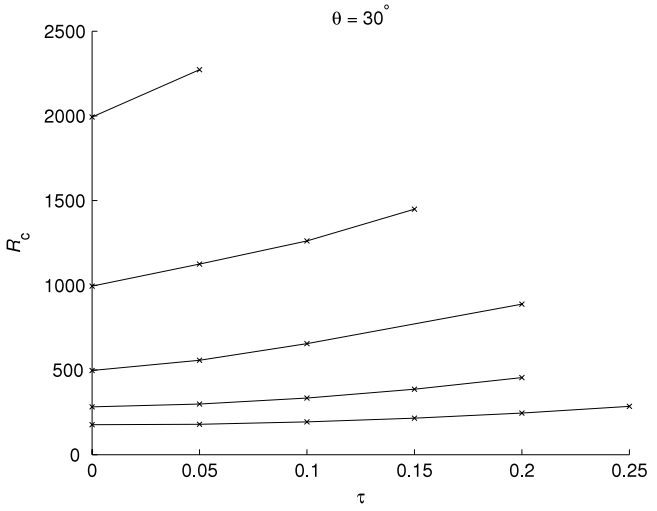

Fig. 9. Critical Reynolds numbers for the onset of convective instability at $\theta = 30°$, for $\iota = -1, -0.5, 0, 0.5, 1$ (leftmost-top to bottom).

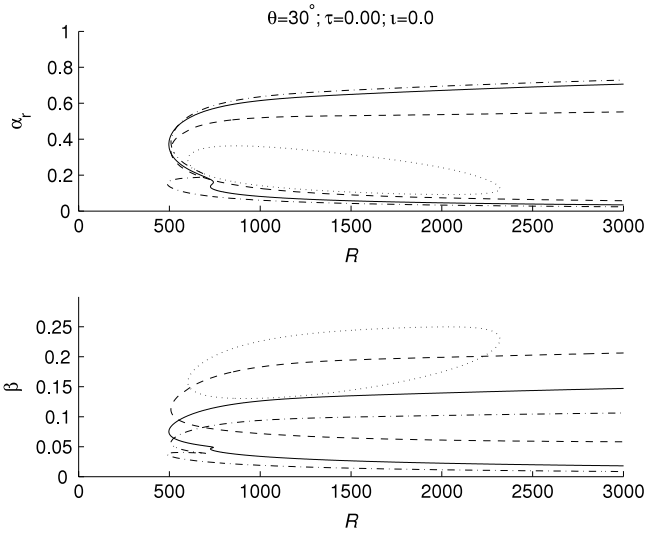

Fig. 10. Neutral-stability curves for $\theta = 30°, \iota = \tau = 0$; $c = 0.7(\cdots)$, $0.8(- -)$, $1(-)$, $1.2(-\cdot-)$.

show good agreement with those of Garrett [14]. Due to the large number of parameters involved, no attempt is made to present all the relevant neutral curves, and instead, only the critical Reynolds numbers are listed. As before, we find that surface suction has a stabilising effect, increasing the critical Reynolds numbers for all parameter values. It also exaggerates the two-lobe profile of the curve. The lobe corresponding to the type II mode is affected more than the type I mode. Once again, surface mass injection has the effect of decreasing the critical Reynolds numbers for all parameter values and is destabilising.

When we examine cases with both forced axial flow and non-zero ι, we see that for large positive ι, increasing the magnitude of forced axial flow has only a modest effect on R_c. However, it broadens the range of wavenumbers over which convective instability is predicted. This effect was observed for stationary vortices, but we now observe that the magnitude of the distortion is highly dependent on the vortex speed, with greater effects apparent for systems with large c; there is very little broadening of the wavenumber range in the slow case of $c = 0.7$.

Although only selected combinations of parameters are presented here, the results show a smooth transition between the extremes of each parameter. In all cases, larger values of c make the

Table 4
R_c for a range of parameter values at $\theta = 10°$.

τ	ι	c				c with lowest R_c
		0.7	0.8	1.0	1.2	
0.0	−1	**9225**	**6810**	6611 (**6309**)	6769 (**3997**)	0.94
	0	**1921**	**1622**	**1601** (2478)	**1650** (1681)	0.90
	1	**641**	**596**	**603**	**625**	0.85
0.2	−1	–	–	–	–	–
	0	*	**2951**	**3005** (3056)	4189 (**1482**)	0.88
	1	**800**	**758**	**845**	1015 (**982**)	0.79

* No unstable region predicted.

Table 5
R_c for a range of parameter values at $\theta = 30°$.

τ	ι	c				c with lowest R_c
		0.7	0.8	1.0	1.2	
0.0	−1	**3257**	**2366**	2272 (**1993**)	2313 (**1249**)	0.96
	0	**602**	**508**	**497** (726)	509 (**488**)	0.93
	1	**190**	**177**	**177**	**181**	0.89
0.2	−1	–	–	–	–	–
	0	*	**933**	937 (**888**)	1257 (**416**)	0.88
	1	**238**	**226**	**246**	281 (**271**)	0.79

* No unstable region predicted.

Table 6
R_c for a range of parameter values at $\theta = 70°$.

τ	ι	c				c with lowest R_c
		0.7	0.8	1.0	1.2	
0.0	−1	**2506**	**1506**	(**421**)	(**243**)	*
	0	**157**	**135**	(**92**)	(**49**)	(1.19)
	1	**41**	**39**	**36**	**34**	*
0.2	−1	–	–	–	–	–
	0	**437**	**275**	**93**	**43**	*
	1	**51**	**50**	**46**	**33**	*

* No minimum within this range of c.

streamline-curvature lobe increasingly significant with respect to the crossflow lobe.

Tables 4–6 provide critical Reynolds numbers for a representative range of parameter values, at selected latitudes. Each entry in the table may contain a pair of critical values: one for the crossflow lobe, and one for the streamline-curvature lobe (in parentheses). If either lobe is not present, its corresponding value is omitted. In all cases, the lower of the two, representing R_c, is given in bold text. As with the previous tables, the absence of data is indicated by a dash. Where the streamline-curvature lobe is present, its critical Reynolds number decreases monotonically with increasing c over the range examined in this work. For the crossflow lobe, however, there is typically a value of c for which the critical Reynolds number is minimised, and this value is given in the rightmost column.

Travelling modes with $c < 1$, which are expected to be dominant on highly polished surfaces, are seen to be more sensitive to both axial flow and surface suction than are stationary modes.

In most cases, the value of c that gives the lowest R_c is less than one. Close to the equator, we can no longer find a minimum in R_c within the range of c examined.

Our formulation means that $-\alpha_i$ can be interpreted as the growth rate of the disturbance. For a selection of cases, we have sampled the maximum growth rate (with respect to α_r) at a Reynolds number of $R_c + 150$. Fig. 11 shows the trends in these results at a latitude of 30°. It is clear that increasing ι increases the growth rate. With $\iota = \tau = 0$, the maximum growth rate is predicted at a disturbance speed of $c = 0.76$, which shows good agreement with the results of Garrett [14], and the data also corroborate his observation that the peak moves to a slightly higher value of c with increased axial flow.

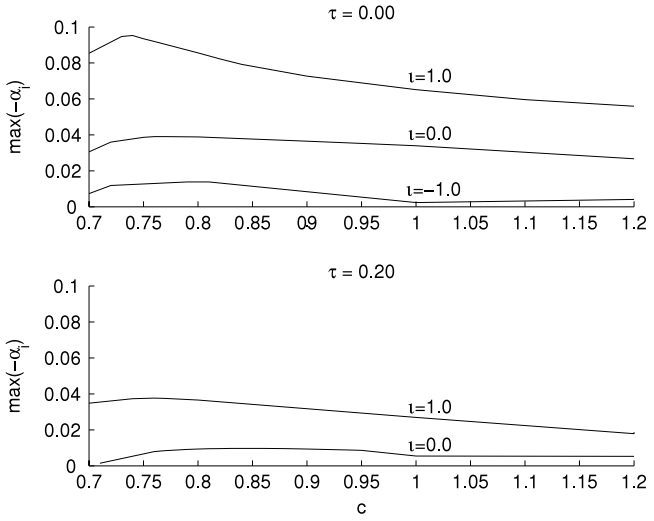

Fig. 11. Spatial growth rates over a range of c at selected τ and ι; $R = R_c + 150$, $\theta = 30°$.

3.2. Absolute instability analysis

We now turn our attention to the occurrence of local absolute instability, where the initial disturbance causes a reaction that is unbounded for large time at all points in space. Prediction of the onset of absolute instability therefore requires the use of a spatio-temporal analysis. This in contrast to the purely spatial analysis that was used to predict convective instability in Section 3.1. While the imaginary part of γ was zero by assumption during the convective analysis, it can no longer be restricted to taking real values; both α and γ are considered to be complex quantities, while β remains real. Furthermore, the concept of disturbance speed does not exist in this context and we revert back to a dispersion relation of the form

$$D(\alpha, \beta, \gamma; R, \theta, \tau, \iota) = 0. \tag{6}$$

Occurrences of uni-directional absolute instability in the latitudinal direction can be found using the Briggs–Bers [21] procedure; they correspond to singularities in the dispersion relation, where spatial branches from opposite sides of the complex α plane "pinch" together. At such a pinch point, the latitudinal complex group velocity, $\partial\gamma/\partial\alpha = 0$. It is necessary for γ_i to be positive at this pinch-point in order to identify absolute instability; if γ_i is negative, any instability is convective. Note that a region of absolute instability must lie within a region of convective instability, and consequently it must hold that $R_a > R_c$ in each case. Also note that absolute instability in the azimuthal direction does not exist within our formulation, owing to the rotational symmetry of the flow.

Unlike the convective neutral-stability curves of previous chapters, neutral curves for absolute instability (where $\gamma_i = 0$) are always single-lobed. The critical Reynolds number for the onset of absolute instability for a given case is denoted by R_a. Again, we examine in detail the case of $\theta = 30°$. Tables 7 and 8 give the value of R_a for several combinations of parameters (combinations for which no data could be obtained are marked with '–'), and Fig. 12 uses the same data to show how R_a is affected by changes in τ and ι. It shows that as ι increases from −1.0 (the topmost line) to 1.0 (the bottommost line), R_a grows less quickly with τ. This suggests that surface suction postpones the onset of absolute instability and that injection promotes it, with a substantially greater effect observed for large magnitudes of forced axial flow. Cases where $\iota = 0$ show excellent agreement with Garrett and Peake [12]. However, the data (which are not presented here) show an increasing discrepancy as θ is increased. We believe that this is due to a slight difference in the steady basic flow profiles used. The results in the current paper are considered to be more reliable.

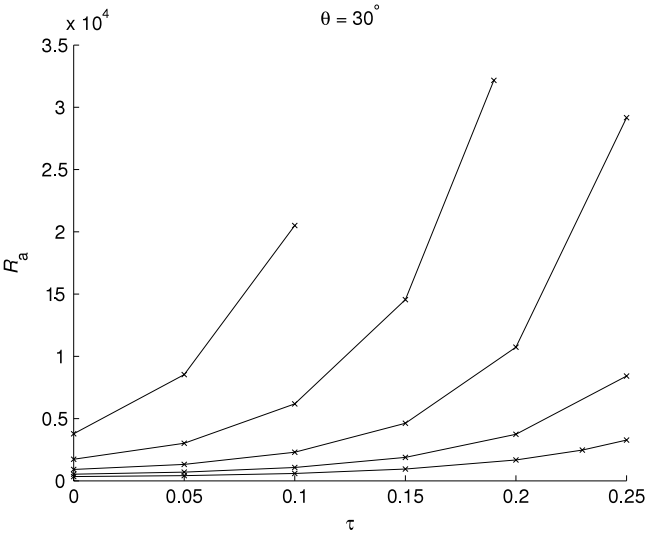

Fig. 12. Critical Reynolds numbers for the onset of absolute instability at $\theta = 30°$; for $\iota = -1, -0.5, 0, 0.5, 1$ (leftmost-top to bottom).

Table 7
R_a at selected latitudes for $\iota = 0.0$.

		τ					
		0.00	0.05	0.10	0.15	0.20	0.25
θ	10°	2883	4198	7420	15,317	36,703	103,663
	30°	913	1321	2299	4,626	10,738	29,165
	50°	482	690	1177	2,299	5,139	13,368
	70°	240	346	578	1,095	2,370	5,989

Table 8
R_a at selected parameter values for $\theta = 30°$.

		τ					
		0.00	0.05	0.10	0.15	0.20	0.25
ι	−1.0	3784	8531	20,509	–	–	–
	−0.5	1735	3017	6,184	14,552	–	–
	0.0	913	1321	2,299	4,626	10,738	29,165
	0.5	535	697	1,072	1,881	3,735	8,418
	1.0	339	417	594	947	1,673	3,276

4. Conclusion

Surface mass suction and injection were seen to have a stabilising and destabilising effect, respectively, upon the flow. There were seen to be two factors involved in understanding the stability of the system: one was the value of R_c, below which no convective instability is predicted; the other was the range of α and β that is susceptible to instability.

Increased axial flow was seen to exaggerate the streamline curvature lobe relative to the crossflow lobe, and in most cases, it significantly increased R_c. However, it typically broadens the range of α and β that support the convectively unstable flow regime, with the greatest effect seen in the position of the top branch.

These effects were observed over the entire range of c that was studied. Models with low vortex speeds were seen to be less sensitive to changes in τ. Lowering c caused the unstable region to shrink or, in some cases, disappear altogether.

In most cases, vortices with $c < 1$ were able to develop at lower Reynolds numbers than stationary disturbances, although this behaviour is less clear close the the equator.

The results demonstrate that surface suction and axial flow typically postpone the onset of both convective and absolute instabilities. This may have implications for the design of turbomachinery and aerospace applications, where maintaining a laminar flow is important for reasons of efficiency. We have shown that surface suction might be used as a flow-control mechanism by creating conditions that delay the onset of convective instability modes (both stationary and travelling) and also the onset of absolute instability.

Acknowledgments

This work was supported by the Engineering and Physical Sciences Research Council (EP/G061637/1) and the University of Leicester.

References

[1] N. Gregory, W.S. Walker, Experiments on the effect of suction on the flow due to a rotating disk, Philos. Trans. R. Soc. Lond. 248 (1960) 225–234.
[2] N. Gregory, W.S. Walker, Experiments on the effect of suction on the flow due to a rotating disk, Rep. Aero. Res. Coun. Lond. 16 (1953) 152.
[3] J.T. Stuart, On the effect of uniform suction on the steady flow due to a rotating disk, Q. J. Mech. Appl. Math. 7 (1954) 446–457.
[4] H. Ockendon, An asymptotic solution for steady flow above an infinite rotating disc with suction, Q. J. Mech. Appl. Math. 25 (1971) 291–301.
[5] M.R. Dhanak, Effects of uniform suction on the stability of flow on a rotating disk, Proc. R. Soc. Lond. Ser. A 439 (1992) 431–440.
[6] A.P. Bassom, S.O. Seddougui, The effects of suction on the nonlinear stability of the three-dimensional boundary layer above a rotating disk, Proc. R. Soc. Lond. Ser. A 436 (1992) 405–415.
[7] R.J. Lingwood, On the effects of suction and injection on the absolute instability of the rotating-disk boundary layer, Phys. Fluids 9 (1997) 1317–1328.
[8] M. Turkyilmazoglu, Lower branch modes of the compressible boundary layer due to a rotating-disk, Stud. Appl. Math. 114 (2005) 17–43.
[9] R.J. Lingwood, S.J. Garrett, The effects of surface mass flux on the instability of the BEK system of rotating boundary-layer flows, Eur. J. Mech. B/Fluids 30 (2011) 299–310.
[10] R.J. Lingwood, Absolute instability of the boundary layer on a rotating disk, J. Fluid Mech. 299 (1995) 17–33.
[11] R.J. Lingwood, An experimental study of absolute instability of the rotating-disk boundary-layer flow, J. Fluid Mech. 314 (1996) 373–405.
[12] S.J. Garrett, N. Peake, The stability and transition of the boundary layer on a rotating sphere, J. Fluid Mech. 456 (2002) 199–218.
[13] S.J. Garrett, N. Peake, The stability of the boundary layer on a sphere rotating in a uniform axial flow, Eur. J. Mech. B Fluids 23 (2004) 241–253.
[14] S.J. Garrett, Vortex-speed selection within the boundary-layer flow over a rotating sphere placed in an enforced axial flow, Eur. J. Mech. B/Fluids 29 (2010) 84–92.
[15] L. Howarth, Note on the boundary layer on a rotating sphere, Phil. Mag. 42 (1951) 1308–1315.
[16] W.H.H. Banks, The boundary layer on a rotating sphere, Q. J. Mech. Appl. Math. 18 (1965) 443–454.
[17] R. Manohar, The boundary layer on a rotating sphere, Z. Angew. Math. Phys. 18 (1967) 320.
[18] W.H.H. Banks, Laminar boundary-layer on a rotating sphere, Acta Mech. 24 (1976) 273–287.
[19] A. Fage, Experiments on a sphere at critical Reynolds numbers, Aero. Res. Council London, R & M 1766 (1936).
[20] S.J. Garrett, The stability and transition of the boundary layer on rotating bodies, Cambridge University, 2002.
[21] R.J. Briggs, Electron-stream Interaction with Plasmas, M.I.T. Press, Cambridge, 1964.
[22] R. Kobayashi, T. Aria, Laminar-turbulent transition, in: Spiral Vortex Behavior in Transition Region and Separation of Three-dimensional Boundary Layers on Spheres Rotating in Axial Flow, in: Proceedings of the IUTAM Symposium, Toulouse, France, Sept. 11–15, 1989 (A91-39901 16-34), Springer-Verlag, Berlin and New York, 1990, pp. 551–557.
[23] S.J. Garrett, Vortex-speed selection within the rotating-disk boundary layer, J. Algorithms Comput. Technol. 4 (2010).